Regionally specific hyperfine polarization of Rb atoms in the vicinity ($\sim 10^{-5}$ cm) of surfaces

K. Zhao and Z. Wu
Department of Physics, Rutgers University, Newark, New Jersey 07102, USA
(Received 15 June 2004; published 19 January 2005)

We made *regionally specific* measurement of the hyperfine polarization $\langle \boldsymbol{S}\cdot\boldsymbol{I}\rangle$ of Rb atoms in the vicinity ($\sim 10^{-5}$ cm) of coated and uncoated Pyrex glass surfaces in optical pumping cells. This is in contrast to the previous hyperfine polarization studies, where the quantity measured is the bulk hyperfine polarization, which depends on surface interactions *averaged over the entire cell surfaces*. We probe the hyperfine polarization of the Rb atoms in the vicinity of cell surfaces using the evanescent wave of a weak laser beam. We find that the polarization in the vicinity of uncoated surfaces is significantly lower than that in the bulk. The polarization decreases rapidly with decreasing distance from the surface. By contrast, the polarization in the vicinity of a silicone-coated Pyrex glass surface is independent of the distance from the cell surface and is equal to the bulk polarization. Regionally specific measurement of the hyperfine polarization as a function of the penetration depth of the evanescent wave allows us to deduce the hyperfine polarization, its normal gradient, as well as the normal gradient coefficient $\mu_{\boldsymbol{S}\cdot\boldsymbol{I}}$ at the cell surface. We present the values of these quantities for three representative uncoated cells.

DOI: 10.1103/PhysRevA.71.012902 PACS number(s): 34.50.Dy, 32.10.Fn, 42.25.Bs

I. INTRODUCTION

Hyperfine polarization of alkali-metal atoms has been studied for decades, partly because of the important role it plays in atomic frequency standards [1,2]. The physical quantity measured in those studies was the bulk hyperfine polarization. Due to surface interactions, the hyperfine polarizations in the vicinity of cell surfaces can be significantly different from that in the bulk and therefore exhibit a large spatial gradient normal to the surface. Since under most experimental conditions the thickness of this surface layer is more than three orders of magnitude smaller than the cell dimension ($\sim$1 cm), the spatial variation of the hyperfine polarization in the vicinity of cell surfaces cannot be studied when one probes the atoms in the bulk, as was done in previous studies. On the other hand, information about hyperfine polarization very close to the cell surfaces is important in, e.g., designing miniature atomic clocks. Furthermore, the bulk hyperfine polarization depends on surface interactions *averaged over the entire cell surfaces* even though surface interactions may vary from place to place on the cell walls. It is therefore desirable to develop a technique that will allow regionally specific measurement of hyperfine polarization at micron/submicron distance from the cell surfaces.

This technique will also be useful in the study of coatings in optical pumping cells. One of the principal relaxation mechanisms of polarized alkali-metal atoms is the surface interactions on cell walls. It is found, however, that if the cell surfaces are coated with saturated paraffins or certain kinds of silicones, the wall relaxation can be significantly reduced, which in turn can greatly enhance the atomic polarization that can be achieved and produce extremely narrow linewidth in atomic spectroscopy [3]. Consequently, coatings have the potential to be of great use in many fields, such as precision atomic measurements, frequency standards, high sensitivity atomic measurements [4], polarized sources and targets, medical imaging [5], etc. Bouchiat and Brossel made an extensive study of the surface relaxation of spin-polarized Rb atoms on paraffin-coated cell walls by studying the gas phase relaxation of spin-polarized Rb atoms [6]. Coatings can also dramatically reduce the surface relaxation rate of spin-polarized inert gas atoms that do not possess a nuclear quadrupole moment such as ^{129}Xe [7,8]. However, the relaxation rate for ^{129}Xe was found to vary widely among similarly coated cells [7]. This mysterious behavior of coatings is not understood and is probably the reason that coatings have not yet found wide use in atomic physics. The main difficulty in studying coatings is the lack of a simple method to quantify the regional quality of coatings, thus making it hard to determine whether a coating is regionally damaged or defective.

Recently, we have made regionally specific measurement of the hyperfine polarization of Rb atoms in the vicinity ($\sim 10^{-5}$ cm) of uncoated and coated Pyrex glass surfaces [9]. The hyperfine polarization near the surfaces is very sensitive to surface interactions, and therefore can be used to characterize the property of surfaces. In silicone-coated optical pumping cells, we have been able to obtain two-dimensional (2D) images of surfaces by measuring the hyperfine polarization at micron or submicron distance from the cell surfaces [10]. The images provide direct evidence for the existence of the so-called "hot spots,"i.e., the defective areas on coated surfaces. The ability to quantify and map the coating quality in optical pumping cells will be helpful in developing coatings of good and reproducible quality.

In this paper, we will report more details of our experimental study of the hyperfine polarization of Rb atoms in the vicinity of uncoated and coated Pyrex glass surfaces [9]. The basic idea of the experiment is to use a strong pump beam to create hyperfine polarization in the Rb vapor and to probe the hyperfine polarization near the surfaces using the evanescent wave of a weak beam. Evanescent wave spectroscopy provides a unique way to study surface interactions of alkali-metal atoms and has been used by several groups [11–16].

The hyperfine polarization $\langle \boldsymbol{S}\cdot\boldsymbol{I}\rangle$, where $\hbar\boldsymbol{S}$ and $\hbar\boldsymbol{I}$ are, respectively, the spins of the electron and the nucleus, is obtained from the following equation:

$$\langle \boldsymbol{S}\cdot\boldsymbol{I}\rangle = \mathrm{Tr}(\boldsymbol{S}\cdot\boldsymbol{I}\rho) = \frac{I(I+1)}{N_a+N_b}\left(\frac{N_a}{g_a}-\frac{N_b}{g_b}\right), \tag{1}$$

where ρ is the density operator of the ground-state Rb atom, and N_a and N_b are, respectively, the population densities of the ground-state hyperfine multiplets of total angular momenta $a=I+1/2$ and $b=I-1/2$, with g_a and g_b being their respective statistical weights. For ^{87}Rb atoms, $I=3/2$ and therefore the ground-state hyperfine multiplets are $a=2, g_a=5$ and $b=1, g_b=3$. When all of the ^{87}Rb atoms are in the multiplet a, $\langle \boldsymbol{S}\cdot\boldsymbol{I}\rangle=0.75$. For ^{85}Rb, $I=5/2$ and therefore $a=3, g_a=7$ and $b=2, g_b=5$. When all of the ^{85}Rb atoms are in the multiplet a, $\langle \boldsymbol{S}\cdot\boldsymbol{I}\rangle=1.25$.

Due to surface interactions, the density operator and consequently $\langle \boldsymbol{S}\cdot\boldsymbol{I}\rangle$ is a function of the distance z from the cell surface. Regionally specific measurement of the hyperfine polarization as a function of the penetration depth of the evanescent wave allows us to determine the normal gradient coefficient μ, which plays an important role in the theory of surface interactions and is defined by

$$\left.\frac{\partial\rho}{\partial n}\right|_{z=0} = \mu\rho(z=0), \tag{2}$$

where $\partial/\partial n = \mathbf{n}\cdot\boldsymbol{\nabla}$ and $\mathbf{n}$ is a unit vector in the direction of the z axis, which is perpendicular to the cell surface (xy plane) and points into the cell. In describing coherent surface interactions, it is essential to treat μ as an operator in Liouville space, acting on the density operator ρ, which is regarded as a vector in Liouville space [17]. Under our experimental conditions, μ is characterized by a scalar $\mu_{\boldsymbol{S}\cdot\boldsymbol{I}}$, which is defined by

$$\mu_{\boldsymbol{S}\cdot\boldsymbol{I}} = \frac{\partial\langle \boldsymbol{S}\cdot\boldsymbol{I}\rangle/\partial n|_{z=0}}{\langle \boldsymbol{S}\cdot\boldsymbol{I}\rangle|_{z=0}}, \tag{3}$$

and will be referred to as the normal gradient coefficient [18].

II. EXPERIMENT AND RESULTS

A. Experiment

The Pyrex glass cells used in the experiment are cylindrical in shape. Their diameters vary from 12 to 30 mm and their lengths from 1.6 to 50.0 mm. The cells contain isotopically enriched Rb (98.3 at. % ^{87}Rb) or Rb of natural abundance. They also contain N_2 buffer gas of various pressures. The pressures refer to 25 °C. We use both coated and uncoated cells. The coating is done using SurfaSil (a siliconizing agent), following a procedure similar to that described in Ref. [19]. For coated cells, care is taken to make sure that coated surfaces are not covered with Rb atoms [6]. This is achieved by the following precautions. (i) Cells are made to have a 90° bent rather than straight stem so that during Rb filling no Rb metal will get into the cell body. (ii) During the experiment, the body of the cell is maintained at temperatures about 10 °C higher than that of the tip where the Rb metal is by placing the tip in a small chamber and flowing room-temperature air through the small chamber. As noted in Ref. [19] and also observed in the present experiment, Rb density in coated cells can be significantly lower than that in uncoated cells. All Rb densities reported here are directly measured rather than inferred from the cell temperature, using the method described in Ref. [20]. The experimental setup is shown in Fig. 1. The Rb cell is mounted inside an oven and heated by flowing hot air into the oven. Cell temperature and the temperature of the tip where the Rb metal is are measured using thermocouples attached to the cell body and the tip. By adjusting the air flow into the small chamber, the temperatures of the tip and the body can be controlled independently to better than 0.2 °C using a feedback system. The oven is mounted on a rotation stage with a resolution of 0.001°. A truncated right angle fused quartz prism is attached to one of the windows of the cell using index matching silicone fluid.

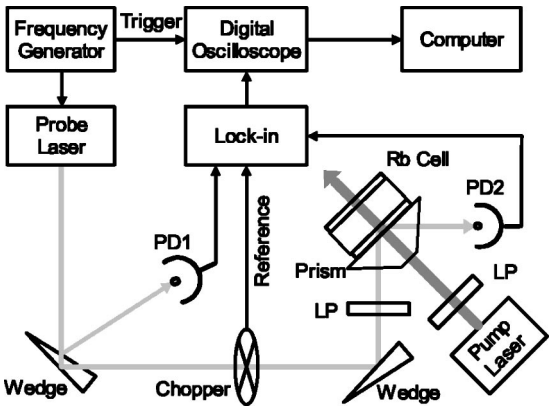

FIG. 1. The experimental setup. PD1 and PD2, silicon photodiodes. LP, Glan-Thompson linear polarizer.

Single-mode diode lasers operated in the free-running mode with a linewidth of 45 MHz and followed by a Glan-Thompson linear polarizer (LP) (extinction ratio of $\sim 10^{-5}$) provide linearly polarized pump and probe beams. Both beams are p-polarized and diffraction limited, with an angular beam spread of 0.025°. The pump beam is incident perpendicularly on the cell surface. Its frequency is tuned to the transitions c_1, d_1 or c_2, d_2, depending on whether the cell is filled with isotopically enriched ^{87}Rb (98.3 at. %) or Rb of natural abundance. The designation of the transitions is indicated in Fig. 2. The transitions c_1 and d_1 are not resolved due to collisional and Doppler broadening. The same is true for the transitions c_2 and d_2. The pump beam depletes the population of the hyperfine multiplet b, causing an accumulation of the Rb atoms in the hyperfine multiplet a.

To use the phase-sensitive detection method, the probe beam is modulated by an optical chopper at a frequency of 1900 Hz. The probe beam has an intensity of 6 μW/cm^2. It is incident at the same spot where the pump is and at an angle slightly larger than the critical angle $\theta_c = \sin^{-1}(1/\sqrt{\epsilon_1}) = \sin^{-1}(1/n_1)$, where ϵ_1 and n_1 are, respectively, the dielectric constant and index of reflection of the glass. The probe beam undergoes total internal reflection at the interface between

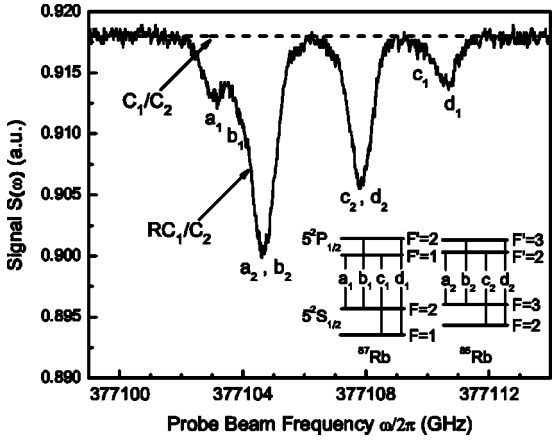

FIG. 2. A representative attenuated total internal reflection signal $S(\omega)$ in a cell filled with Rb metal of natural abundance and 5 Torr N_2. The Rb density is 2.76×10^{13} cm^{-3}. The incidence angle of the probe beam corresponds to a penetration depth of 0.51 μm. The signal is averaged 10 times. The dashed line corresponds to no absorption and therefore is equal to C_1/C_2. The reflectivity $\mathcal{R}(\omega)$ is obtained by dividing the signal $\mathcal{R}(\omega)C_1/C_2$ by the dashed line C_1/C_2.

the Pyrex glass and Rb vapor. The size of the probe beam is sufficiently smaller than that of the pump beam so that it can be completely overlapped by the pump beam. The frequency of the probe beam is scanned across the Rb $D1$ line. The reflectivity $\mathcal{R}(\omega)$ of the probe beam is measured using the following method. A photodiode PD1 measures the intensity of the reflected probe beam. Its output is given by $C_1 I_{\text{laser}}(\omega)\mathcal{R}(\omega)$, where $I_{\text{laser}}(\omega)$ is the output intensity of the probe laser and C_1 takes care of the reflectivity and transmissivity of various optical components such as linear polarizer, wedges, windows of the oven, prism surfaces, etc. The output of P1 is fed into a lock-in amplifier. The intensity of the laser beam is monitored by a second photodiode PD2, the output of which is equal to $C_2 I_{\text{laser}}(\omega)$, with C_2 having a similar meaning to C_1, and is fed into the same lock-in to divide the output of P1, so that any intensity change or fluctuation of the laser beam during the frequency scan is canceled out. The output of the lock-in is therefore given by

$$S(\omega) = \frac{C_1}{C_2}\mathcal{R}(\omega), \tag{4}$$

which is obviously independent of laser intensity. A typical total internal reflection signal is shown in Fig. 2, and the procedure for obtaining the reflectivity $\mathcal{R}$ from the data is explained in the caption of Fig. 2.

Since no wavemeter is used in the laser frequency scan to correlate time and laser frequency, signals are recorded on the oscilloscope as a function of time rather than frequency. The conversion of the time base to the absolute frequency base is done as follows. The probe beam is allowed to pass through a reference cell filled with Rb metal and no buffer gas. The absorption spectra are taken in the same way as the reflectivity $\mathcal{R}(\omega)$ so that the recorded reflectivity $\mathcal{R}(\omega)$ and absorption spectra have the same time base. Since the cell is maintained at 25 °C when absorption spectra are taken, all the transition frequencies $\omega_{FF'}$ can be assumed to be unshifted. By comparing the absorption spectra with the known frequencies of the transitions between the hyperfine multiplets of the ground and excited states of Rb [21], one can convert the time base of the recorded reflectivity $R(\omega)$ into an absolute frequency base.

B. Average hyperfine polarization $\overline{\langle \boldsymbol{S}\cdot\boldsymbol{I}\rangle}$

Experimental study is done in two types of cells: cells filled with isotopically enriched Rb (98.3 at. % ^{87}Rb) and those filled with Rb of natural abundance. Since the experimental methods and results are similar for these two types of cells, we will focus on the study of ^{87}Rb, briefly mentioning the differences that may arise for the cells filled with natural Rb. In cells filled with isotopically enriched Rb (98.3 at. % ^{87}Rb), the N_2 pressure is 25 Torr. We choose this pressure to insure that the transitions c_1 and d_1 have sufficient overlap. In these cells, the ^{85}Rb atoms make little contribution to the signal except at high cell temperatures and in the study of bulk hyperfine pumping. The pump beam is tuned to the transitions c_1 and d_1. The ^{87}Rb hyperfine polarization $\langle \boldsymbol{S}\cdot\boldsymbol{I}\rangle$ in the vicinity of cell surfaces is obtained from Eq. (1). Therefore, one needs to know the population densities N_a and N_b near the cell surfaces. Due to surface relaxation, however, the population densities and consequently the hyperfine polarization in the vicinity of surfaces are functions of z. A convenient way to study the z dependence of the hyperfine polarization $\langle \boldsymbol{S}\cdot\boldsymbol{I}\rangle$ is to introduce the average hyperfine polarization $\overline{\langle \boldsymbol{S}\cdot\boldsymbol{I}\rangle}$, which for a given penetration depth d is obtained by replacing $N_a(z)$ and $N_b(z)$ by their average values $\overline{N_a}$ and $\overline{N_b}$. Here the penetration depth d of the probe beam is defined by

$$d = \frac{\lambda_0}{2\pi}\frac{1}{\sqrt{\epsilon_1 \sin^2\theta - 1}}, \tag{5}$$

with λ_0 being the wavelength of the beam in the vacuum. The average population densities $\overline{N_a}$ and $\overline{N_b}$ are determined as the fitting parameters that give the best fit between the measured reflectivity $\mathcal{R}(\omega)$ and the calculated one. The details for the calculation of $\mathcal{R}(\omega)$ and the determination of $\overline{N_a}$ and $\overline{N_b}$ are described in the Appendix (see Appendix A 4 a and A 4 d). The z dependence of the actual population densities N_a and N_b manifests itself in the dependence of the average population densities $\overline{N_a}$ and $\overline{N_b}$ on the penetration depth d (Fig. 3).

The values of $\overline{N_a}$ and $\overline{N_b}$ thus determined are used in Eq. (1) to compute the average hyperfine polarization $\overline{\langle \boldsymbol{S}\cdot\boldsymbol{I}\rangle}$. Figure 4 displays the dependence of the average hyperfine polarization $\overline{\langle \boldsymbol{S}\cdot\boldsymbol{I}\rangle}$ on the penetration depth d in some representative coated and uncoated cells. It is important to note that the average hyperfine polarization near the cell surfaces as plotted in Fig. 4 is regionally specific rather than averaged over the entire cell surfaces. That is, the measured average hyperfine polarization is determined by the *regional* surface interactions. The spatial resolution of the hyperfine polariza-

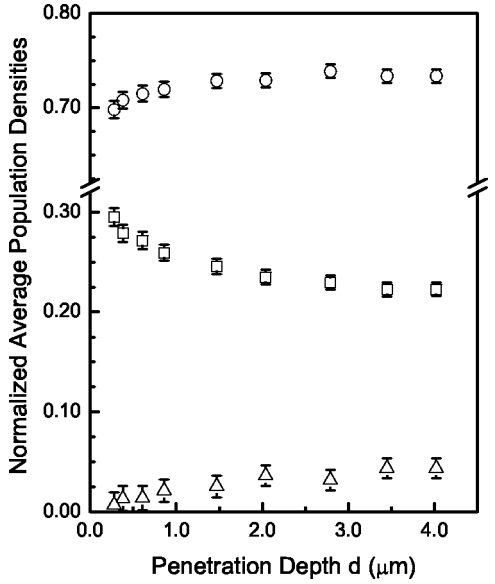

FIG. 3. The dependence of the normalized average population densities $\overline{N_a}/N$ (○) and $\overline{N_b}/N$ (□) on the penetration depth d in a representative uncoated cell (no. 17). The cell contains isotopically enriched Rb (98.3 at. % ^{87}Rb) and 25 Torr N_2. The Rb density is 6.2×10^{13} cm^{-3}. The pump beam intensity is 1.3 W/cm^2. The average excited-state population $\overline{N_e}/N$ (△), which constitutes a few percent of the total population, is also indicated (see Appendix A 4 a).

tion in the xy plane is determined in the present experiment by the size of the probe beam, which is about 1.0 mm [10]. In the coated cell, the dependence of the average hyperfine polarization on the penetration depth is studied for two different pumping intensities 1.3 W/cm^2 and 8 mW/cm^2. At 1.3 W/cm^2 pumping intensity, the average hyperfine polarization is 0.70 ± 0.02 and is independent of the penetration depth within experimental uncertainties. That is, the Rb vapor is almost fully polarized all the way to the cell surface. For pumping intensity 8 mW/cm^2, although the average hyperfine polarization is substantially smaller (0.32 ± 0.02), it is still independent of the distance from the cell surfaces. This is in sharp contrast with the uncoated cells, in which the average hyperfine polarization near the surfaces is significantly smaller than that in the bulk. The distance over which the average hyperfine polarization changes rapidly is on the order of 10^{-3} cm. Thus, we come to the conclusion that in the vicinity of uncoated surfaces, the relaxation rate of hyperfine polarization is dominated by surface interactions whereas the relaxation rate near coated surfaces is still dominated by bulk interactions such as collisions with Rb atoms and buffer gas molecules.

Shown in Fig. 5 and 6 are the typical data of ^{87}Rb hyperfine pumping in the vicinity of cell surfaces in coated and uncoated cells. In spite of its narrow linewidth, the pump beam pumps all velocity groups as a result of collision broadening and velocity-changing collisions [22]. This is also confirmed by the hyperfine pumping data in Figs. 5 and 6. For comparison, bulk hyperfine pumping data taken in the same coated and uncoated cells under the same experimental conditions are also shown. The method of obtaining the average bulk hyperfine polarization is similar to that used to obtain the average surface hyperfine polarization. The only difference is that the probe beam, instead of undergoing total internal reflection, passes through the cell and the transmissivity as a function of the probe beam frequency is measured. Details are given in Appendix A 4 b and A 4 d. Numerically calculated reflectivity $\mathcal{R}(\omega)$ and transmissivity $\mathcal{T}(\omega)$ are also shown in Fig. 5 and Fig. 6. The fit is excellent.

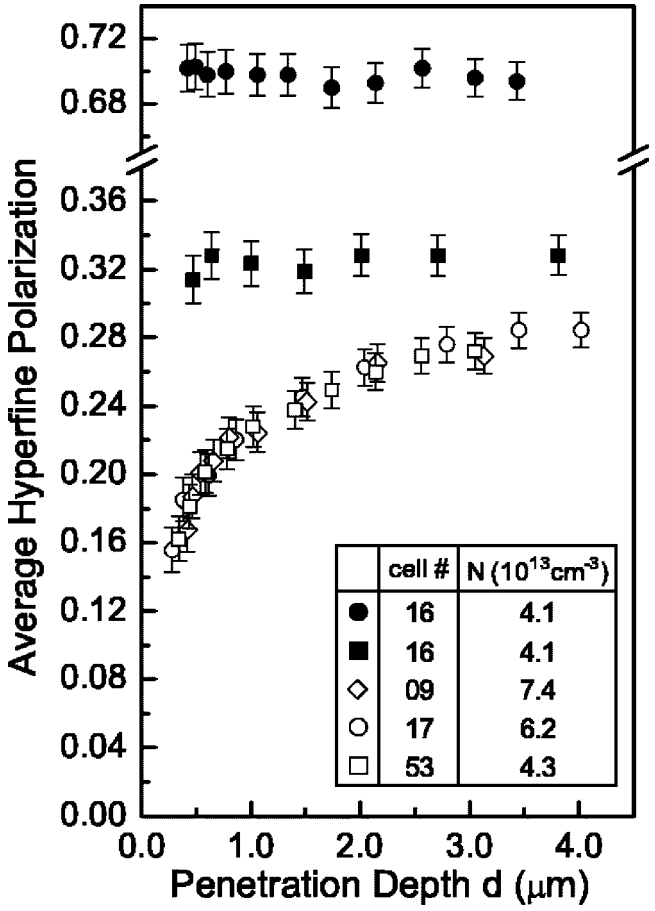

FIG. 4. The dependence of the average hyperfine polarization $\overline{\langle \boldsymbol{S}\cdot\boldsymbol{I}\rangle}$ on the penetration depth d in a coated (●, ■) and three uncoated (○, □, ◇) cells filled with isotopically enriched Rb (98.3 at. % ^{87}Rb) and 25 Torr N_2. The Rb density for each cell is indicated in the legend. The pump beam intensity is 8 mW/cm^2 for the ■ data and 1.3 W/cm^2 for all the other data. The uncertainty in the penetration depth due to the diffraction limit of the probe laser beam is not shown in the figure.

We note that the average hyperfine polarization $\overline{\langle \boldsymbol{S}\cdot\boldsymbol{I}\rangle}$ in Fig. 4 does not seem to be approaching the bulk value ($\sim$0.7) as d increases. To understand this, we made a simulation study, which allows us to study the average hyperfine polarization for large values of d that would otherwise be difficult to achieve experimentally due to the diffraction limit of the probe beam.

The penetration depth d as defined by Eq. (5) does not depend on the frequency of the probe beam, and therefore serves as a convenient frequency-independent length scale. Physically, it represents the $1/e$ decay distance of the amplitude of the evanescent wave when the frequency of the probe

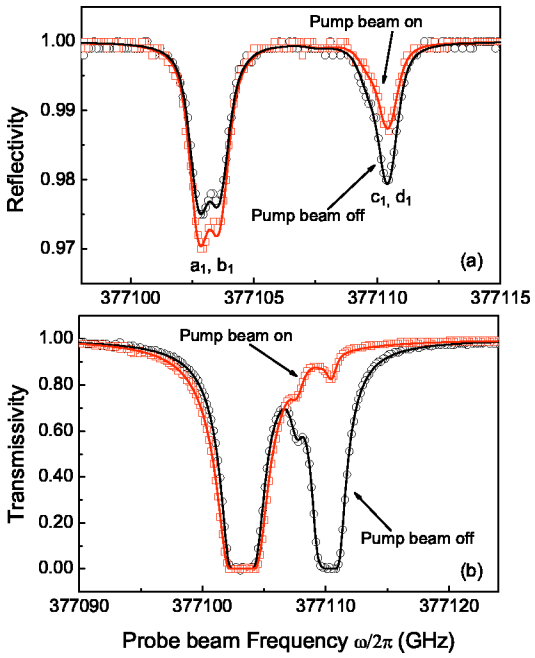

FIG. 5. (Color online) Comparison of the hyperfine pumping near the surface (a) and in the bulk (b) in an uncoated ^{87}Rb cell (no. 9) with 25 Torr N_2. The temperature is 100.0 °C and the Rb density is 5.8×10^{12} cm^{-3}. The pump beam intensity is 1.3 W/cm^2. The incidence angle of the probe beam corresponds to a penetration depth of 3.8 μm in (a) while the path length of the probe beam in (b) is 8.75 mm. The evanescent probe beam is perpendicular to the pump beam in (a) whereas the probe and pump beams are parallel to each other in (b). However, the hyperfine pumping in the bulk is independent of the relative orientation of the pump and probe beams due to velocity-changing collisions. The circles and squares are the experimental data and the lines are numerical calculations. From the data, we obtain $\langle \boldsymbol{S}\cdot\boldsymbol{I}\rangle = 0.73\pm0.02$ for the bulk and 0.28 ± 0.01 near the uncoated cell surfaces.

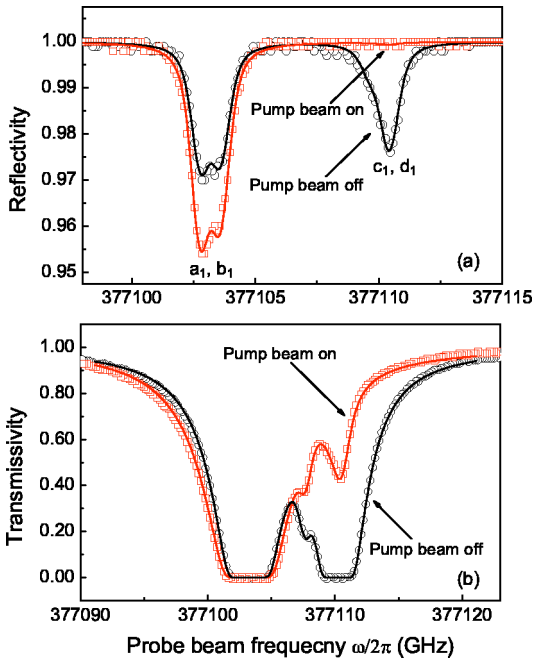

FIG. 6. (Color online) Comparison of the hyperfine pumping near the surface (a) and in the bulk (b) in a coated ^{87}Rb cell (no. 16) with 25 Torr N_2. The Rb density is 7.55×10^{12} cm^{-3}. The pump beam intensity is 1.3 W/cm^2. The incidence angle of the probe beam corresponds to a penetration depth of 3.4 μm in (a). The path length of the probe beam in (b) is 2.0 cm. The circles and squares are the experimental data and the lines are numerical calculations. From the data we obtain $\langle \boldsymbol{S}\cdot\boldsymbol{I}\rangle = 0.72\pm0.02$ for the bulk and 0.73 ± 0.02 near the coated cell surfaces.

beam is far away from the resonance frequencies of the Rb atoms so that the dielectric constant ϵ_2 of the Rb vapor is approximately unity. When the frequency of the probe beam is near the resonance frequencies of the Rb atoms, the dielectric constant of the Rb vapor becomes a frequency-dependent complex number. As a result, the penetration depth also depends on the frequency of the probe beam and will be denoted as d_ω. As will be discussed below, d_ω can be significantly different from the frequency-independent penetration depth d.

If the Rb vapor can be treated as a homogeneous medium with a frequency-dependent complex dielectric constant $\epsilon_2 = \epsilon_2' + i\epsilon_2''$, the penetration depth d_ω of the probe beam is equal to the reciprocal of the imaginary part of $k_z^{(2)}$, the z component of the wave vector $\mathbf{k}^{(2)}$ in the Rb vapor, and can be written as [see Eq. (A6)]

$$d_\omega = \frac{1}{k_0[(\varepsilon_1 \sin^2\theta - \varepsilon_2')^2 + \varepsilon_2''^2]^{1/4}\sin\alpha_2}, \tag{6}$$

where k_0 is the wave vector of the probe beam in the vacuum and α_2 is defined by

$$\tan 2\alpha_2 = \frac{\varepsilon_2''}{\varepsilon_2' - \varepsilon_1 \sin^2\theta}. \tag{7}$$

During hyperfine pumping, however, the Rb vapor near the cell surface needs to be treated as a stratified medium and the penetration depth d_ω can be calculated using the stratified medium theory described in the Appendix (see Appendix A 4 c).

Simulation is done for a cell filled with isotopically enriched Rb (98.3 at. % ^{87}Rb) and 25 Torr N_2. The Rb density is assumed to be 4.7×10^{13}cm^{-3}. During hyperfine pumping the dielectric constant ϵ_2 of the Rb vapor near the surface is given by Eq. (A37) and depends on the population densities $N_a(z)$ and $N_b(z)$ near the surface. For simulation purpose, we use the following linear population density profiles for $N_a(z)$ and $N_b(z)$:

$$\tilde{N}_a(z) = \begin{cases} N_a(0) + [N_a^{(0)} - N_a(0)]z/L, & 0 \le z \le L \\ N_a^{(0)}, & z > L \end{cases}, \tag{8}$$

$$\tilde{N}_b(z) = \begin{cases} N_b(0) + [N_b^{(0)} - N_b(0)]z/L, & 0 \le z \le L \\ N_b^{(0)}, & z > L \end{cases}. \tag{9}$$

The parameters $N_a^{(0)}$ and $N_b^{(0)}$ are the bulk population densities and are chosen to be $0.99N$ and $0.01N$, respectively, where N is the ^{87}Rb density. This choice of $N_a^{(0)}$ and $N_b^{(0)}$

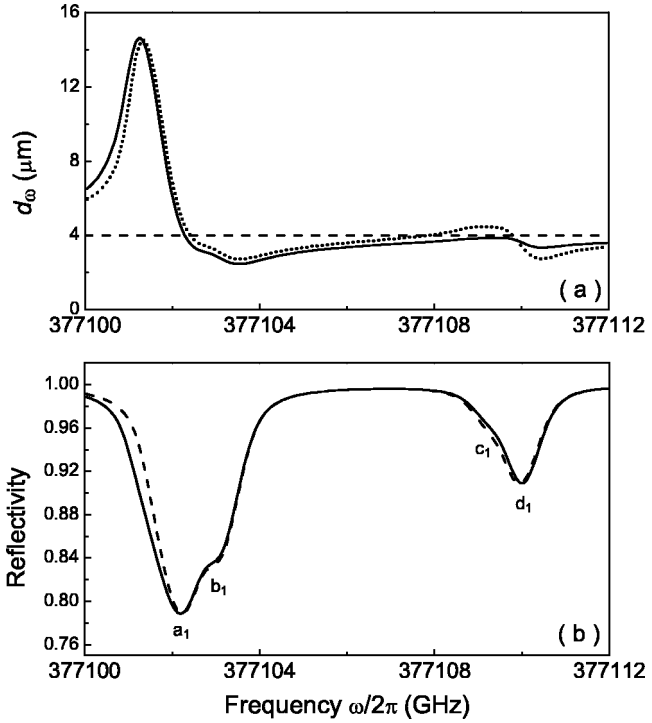

FIG. 7. (a) The penetration depth d_ω vs ω for an incidence angle that corresponds to $d=4.0$ μm (dashed horizontal line). The solid line is the penetration depth for the magnetic field and the dotted line for the electric field. Details of the calculation are described in section Appendix A 4 c. (b) The calculated reflectivity $\mathcal{R}(\omega)$ (solid line) and the fit (dashed line) using the average population densities $\overline{N_a}$ and $\overline{N_b}$ as fitting parameters. One sees that a better fit to the left wing of the transition a_1 requires larger average population density $\overline{N_a}$. Physically, this is due to the larger penetration depth d_ω for frequencies of the red wing of the a_1 peak.

corresponds to a bulk hyperfine polarization of 0.73. The parameters $N_a(0)$ and $N_b(0)$ are the population densities at the surface, and are chosen to be $0.625N$ and $0.375N$, respectively, which corresponds to zero surface hyperfine polarization. The parameter L describes the scale of the length over which the population densities $N_a(z)$ and $N_b(z)$ vary and is chosen to be 4.0 μm. Plotted in Fig. 7(a) is the penetration depth d_ω vs ω for an incidence angle that corresponds to $d=4.0$ μm. The penetration depth d_ω refers to the $1/e$ decay distance for the electric field (see Appendix A 4 c). We note that although d_ω does not deviate significantly from d when ω is larger than ω_{21}, the frequency of a_1 peak, it can be as large as 14.6 μm for frequencies of the red wing of the a_1 peak. Here $\omega_{FF'}$ is the frequency associated with the transition $F\rightarrow F'$, with F and F' representing the hyperfine multiplets of the ground state $5\,^2S_{1/2}$ and the excited state $5\,^2P_{1/2}$, respectively.

Shown in Fig. 7(b) is the reflectivity $\mathcal{R}(\omega)$ calculated using the population densities $\tilde{N}_a(z)$ and $\tilde{N}_b(z)$ in Eqs. (8) and (9). Also shown is the fit using the average population densities $\overline{N_a}$ and $\overline{N_b}$ as fitting parameters. It is seen that for $\omega \geqslant \omega_{21}$ the fit is reasonably good, but for $\omega < \omega_{21}$ the fit is bad. That is, the average hyperfine polarization approximation starts to break down in this frequency range.

Thus we come to the conclusion that the average hyperfine polarization approximation is valid if d_ω has a weak dependence on ω or if $d_\omega \gg L$ over the entire scanned frequency range, where L is the dimension of the surface layer in which the population densities $N_a(z)$ and $N_b(z)$ change from the surface values to the bulk ones. Neither of these criteria is satisfied for the simulation data in Fig. 7(b), which explains the unsatisfactory fit of $\mathcal{R}(\omega)$ using average population densities $\overline{N_a}$ and $\overline{N_b}$.

That the average hyperfine polarization $\overline{\langle \boldsymbol{S}\cdot\boldsymbol{I}\rangle}$ in Fig. 4 does not seem to be approaching the bulk value ($\sim$0.7) as d increases is due to the following two reasons. (i) When d is sufficiently small, it agrees with d_ω and therefore represents the actual penetration depth of the evanescent wave. For example, in our simulation, when $d=1.50$ μm, d_ω lies between 1.40 and 1.65 μm for the entire scanned frequency range. As d increases, for the frequency range $\omega > \omega_{21}$, d_ω lags d more and more until d starts to lose its physical meaning as a measure of the actual distance the evanescent wave travels into the Rb vapor. For example, for $\omega > \omega_{21}$, d_ω lies between 3.2 and 7.4 μm for $d=7.0$ μm, and between 3.3 and 13 μm for $d=80$ μm. (ii) As d increases, the average hyperfine polarization approximation starts to break down due to the larger and larger variation of d_ω over the scanned frequency range. Indeed, for the data shown in Fig. 4 that correspond to $d\sim 4$ μm, the fit between the measured reflectivity and the one calculated using average population densities is noticeably not as good as the fit for $d \lesssim 1$ μm, indicative of the onset of breaking down of the average hyperfine polarization approximation.

The penetration depth d_ω also depends on the Rb density. The higher the Rb density, the larger the discrepancy between d_ω and d. For example, if $d=4$ μm, we find that for the scanned frequency range, d_ω varies between 2.6 and 14.6 μm for Rb density 4.7×10^{13} cm^{-3} and between 3.4 and 4.4 μm for Rb density 5.8×10^{12} cm^{-3}. This is probably the reason that the reflectivity $\mathcal{R}(\omega)$ measured at relatively low Rb densities can still be fitted quite well using average population densities even though d is relatively large ($\sim$4 μm) (see Fig. 5).

For the cells that are filled with natural Rb metal, we choose a N_2 pressure of 5 Torr so that there is sufficient overlap between the transitions c_2 and d_2 and at the same time the overlap between the unsolved peaks a_2,b_2 and c_2,d_2 is negligible. In these cells, the hyperfine pumping is performed on ^{85}Rb. The pump beam is tuned to the transitions c_2 and d_2. The procedure for obtaining the average hyperfine polarization $\overline{\langle \boldsymbol{S}\cdot\boldsymbol{I}\rangle}$ for ^{85}Rb is the same as that used for ^{87}Rb. We note that because the transitions c_1,d_1 and c_2,d_2 overlap in the far wing, the pump beam also produces a small amount of ^{87}Rb hyperfine polarization, which under our experimental conditions is negligible in uncoated cells [see Fig. 8(a)] and about 10% in coated cells [see Fig. 8(b)]. Therefore, for ^{85}Rb hyperfine pumping in coated cells, a small deviation of the ^{87}Rb populations in the ground-state hyperfine levels from their equilibrium values (i.e., when the pump beam is off) needs to be taken into account in order to obtain a good fit between the measured reflectivity and the calculated one.

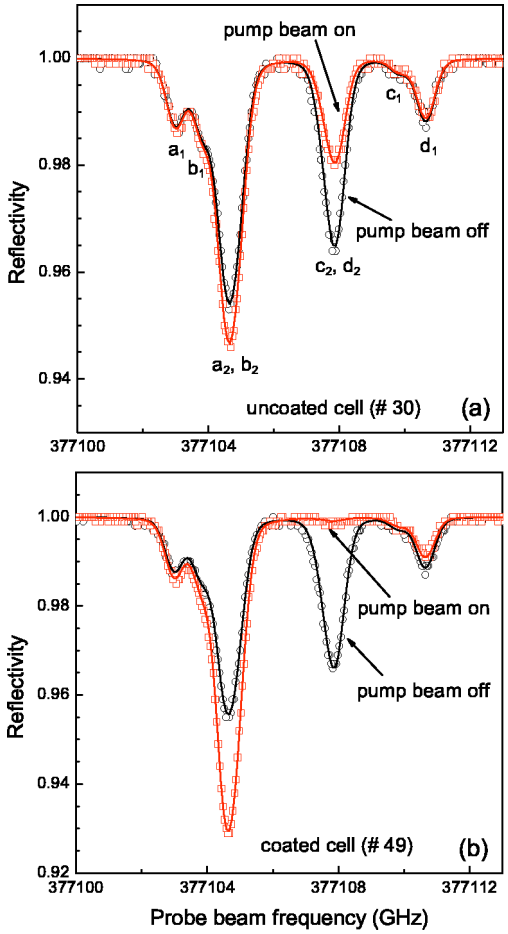

FIG. 8. (Color online) Hyperfine pumping near the cell surfaces in an uncoated and a coated cell filled with Rb of natural abundance and 5 Torr N_2. The Rb density is 2.76×10^{13} cm^{-3} in the uncoated cell and 2.92×10^{13} cm^{-3} in the coated cell. The incidence angle of the probe beam corresponds to a penetration depth of 1.06 μm in (a) and 0.98 μm in (b). The circles and squares are the experimental data and the lines are numerical calculations. From the data we obtain $\overline{\langle \boldsymbol{S}\cdot\boldsymbol{I}\rangle}=0.47$ near uncoated and 1.20 near coated surfaces.

C. Normal gradient coefficient

In this section, we will show that the normal gradient coefficient $\mu_{\boldsymbol{S}\cdot\boldsymbol{I}}$ can be determined by the reflectivity data. For clarity purpose, we will focus on the cells filled with isotopically enriched Rb (98.3 at. % ^{87}Rb). The normal gradient coefficient $\mu_{\boldsymbol{S}\cdot\boldsymbol{I}}$ is defined by Eq. (3). Therefore, one needs to determine the values as well as the normal gradients of $N_a(z)$ and $N_b(z)$ at the surface ($z=0$). The values of $N_a(z)$ and $N_b(z)$ at the surface, $N_a(0)$ and $N_b(0)$, are obtained from the hyperfine polarization at the surface $\langle \boldsymbol{S}\cdot\boldsymbol{I}\rangle|_{z=0}$, which in turn is obtained by extrapolating $\overline{\langle \boldsymbol{S}\cdot\boldsymbol{I}\rangle}$ to $d=0$,

$$\langle \boldsymbol{S}\cdot\boldsymbol{I}\rangle|_{z=0}=\lim_{d\to 0}\overline{\langle \boldsymbol{S}\cdot\boldsymbol{I}\rangle}. \tag{10}$$

The normal gradients of $N_a(z)$ and $N_b(z)$ at the surface ($z=0$) require knowledge of the population density functions $N_a(z)$ and $N_b(z)$ in the vicinity of surfaces, which, however, are unknown. Therefore, we use the following linear approximation method to determine $\partial N_a/\partial n|_{z=0}$ and $\partial N_b/\partial n|_{z=0}$. We measure the reflectivities $\mathcal{R}(\omega)$ for a number of different penetration depths d. Because of the z dependence of N_a, N_b and consequently the dielectric constant ϵ_2, the Rb vapor in the vicinity of cell surfaces needs to be treated as a stratified medium, and the reflectivity $\mathcal{R}(\omega)$ depends on the unknown functions $N_a(z)$ and $N_b(z)$ (see the Appendix). For each penetration depth d of the probe beam, we construct the piecewise linear population density profiles as defined by Eqs. (8) and (9), and adjust the parameter L to give the best fit between the reflectivity $\mathcal{R}(\omega)$ calculated using the population densities $\tilde{N}_a(z)$ and $\tilde{N}_b(z)$ and the measured $\mathcal{R}(\omega)$ which corresponds to the actual population densities $N_a(z)$ and $N_b(z)$. The reason for constructing these linear population density profiles is that, as the penetration depth d of the probe beam approaches zero, the linear population density profiles $\tilde{N}_a(z)$ and $\tilde{N}_b(z)$ approach the respective tangents to the actual population density profiles $N_a(z)$ and $N_b(z)$ at $z=0$ (Fig. 9). The polarization $\widetilde{\langle \boldsymbol{S}\cdot\boldsymbol{I}\rangle}$ that corresponds to the population densities $\tilde{N}_a(z)$ and $\tilde{N}_b(z)$ is also a linear function of z, and becomes the tangent to the polarization $\langle \boldsymbol{S}\cdot\boldsymbol{I}\rangle$ at $z=0$ in the limit of $d\to 0$. That is, we have

$$\left.\frac{\partial\langle \boldsymbol{S}\cdot\boldsymbol{I}\rangle}{\partial n}\right|_{z=0}=\lim_{d\to 0}\frac{\widetilde{\langle \boldsymbol{S}\cdot\boldsymbol{I}\rangle}|_{z=L}-\widetilde{\langle \boldsymbol{S}\cdot\boldsymbol{I}\rangle}|_{z=0}}{L}. \tag{11}$$

The method described above is used to deduce the normal gradient coefficient $\mu_{\boldsymbol{S}\cdot\boldsymbol{I}}$ from a set of reflectivity data $\mathcal{R}(\omega)$ taken at various incidence angles in a representative uncoated cell (cell no. 53) at a Rb density 4.3×10^{13} cm^{-3}. The pump beam intensity is 1.3 W/cm^2. The bulk population densities $N_a^{(0)}$ and $N_b^{(0)}$ are obtained from the bulk transmissivity measurement (see Appendix A 4 b). Substituting the values of $N_a^{(0)}$ and $N_b^{(0)}$ in Eq. (1), we find the bulk polarization

$$\widetilde{\langle \boldsymbol{S}\cdot\boldsymbol{I}\rangle}|_{z=L}=0.70\pm0.02. \tag{12}$$

As mentioned above, the values of $N_a(0)$ and $N_b(0)$ are obtained using extrapolation from the limit $\lim_{d\to 0}\overline{\langle \boldsymbol{S}\cdot\boldsymbol{I}\rangle}$.

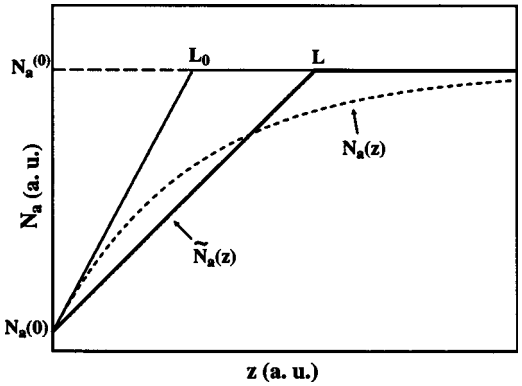

FIG. 9. The limit process used in this study to obtain the slope of $N_a(z)$ at $z=0$. The same process is used to obtain the slope of $N_b(z)$ at $z=0$.

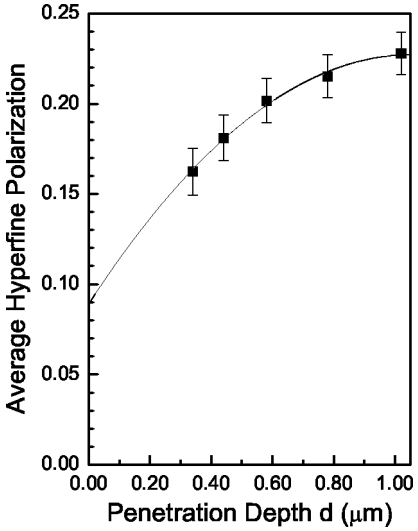

FIG. 10. Expanded plot of the average hyperfine polarization data taken in cell no. 53 that correspond to $d \lesssim 1$ μm (see Fig. 4). The solid line is the extrapolation using a quadratic polynomial fit. The intercept yields the hyperfine polarization at the cell surface $\langle \boldsymbol{S} \cdot \boldsymbol{I} \rangle|_{z=0} = 0.088$.

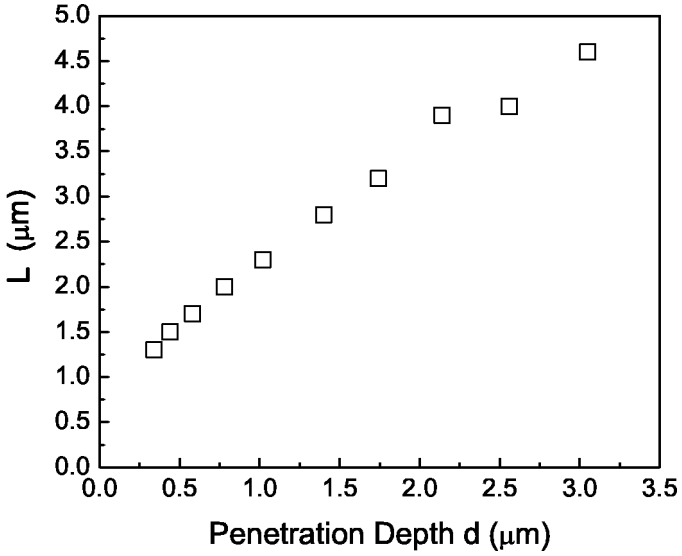

FIG. 11. The dependence of the fitting parameter L on the penetration depth d in the representative uncoated cell no. 53. The extrapolation of L to $d=0$ is done for the data points that correspond to $d \lesssim 1$ μm and yields the intercept $L_0 = 0.84$ μm.

Since, as discussed in Sec. II B, the value of d represents the actual $1/e$ decay distance only for small d and furthermore the average hyperfine polarization approximation is more reliable for small values of d, only the average hyperfine polarization data corresponding to $d \lesssim 1$ μm are used in the extrapolation, which is done using a quadratic polynomial fit as shown in Fig. 10 for cell no. 53. We obtain

$$\langle \boldsymbol{S} \cdot \boldsymbol{I} \rangle|_{z=0} = 0.088, \tag{13}$$

whence

$$\langle \widetilde{\boldsymbol{S} \cdot \boldsymbol{I}} \rangle|_{z=0} = \langle \boldsymbol{S} \cdot \boldsymbol{I} \rangle|_{z=0} = 0.088. \tag{14}$$

For different penetration depths d, we find that L decreases with d and by extrapolating to $d=0$ we obtain the intercept (see Fig. 11)

$$L_0 = 0.84 \ \mu\text{m}. \tag{15}$$

Using Eqs. (12), (14), and (15), we obtain from Eq. (11)

$$\left. \frac{\partial \langle \boldsymbol{S} \cdot \boldsymbol{I} \rangle}{\partial n} \right|_{z=0} = 0.73 \ \mu\text{m}^{-1}. \tag{16}$$

Finally, substituting Eqs. (13) and (16) in Eq. (3), we obtain

$$\mu_{\boldsymbol{S}\cdot\boldsymbol{I}} = 8.3 \ \mu\text{m}^{-1} \tag{17}$$

for the representative uncoated cell no. 53. We did not assign uncertainty to the normal gradient coefficient $\mu_{\boldsymbol{S}\cdot\boldsymbol{I}}$. This is because the values of the hyperfine polarization at the surface $\langle \boldsymbol{S} \cdot \boldsymbol{I} \rangle|_{z=0}$ and the parameter L_0 are obtained using extrapolation, and errors due to extrapolation are difficult to estimate. The physical meaning of the length L_0 is that if the normal gradient $\partial \langle \boldsymbol{S} \cdot \boldsymbol{I} \rangle / \partial n$ in the vicinity of the surface were constant and equal to that at the surface, the hyperfine polarization $\langle \boldsymbol{S} \cdot \boldsymbol{I} \rangle$ would increase from its value at the surface to the bulk value over a distance L_0. The physical meaning of $\mu_{\boldsymbol{S}\cdot\boldsymbol{I}}$ is that if the cell surface were displaced backward a distance $1/\mu_{\boldsymbol{S}\cdot\boldsymbol{I}}$ and the normal gradient of polarization at $z=0$ were to extend uniformly to the displaced surface, the polarization would be zero at the displaced surface. We note that this is in exact analogy with the concept of velocity slip or temperature jump in gas kinetic theory [23].

We did similar studies in two other uncoated cells (no. 09 and no. 17). The results for all three cells are presented in Table I. The hyperfine polarization, its normal gradient, and normal gradient coeeficient at the cell surface in cell no. 09 were reported in Ref. [9], where a different method was used to find the hyperfine polarization at the surface and therefore slightly different values of $\langle \boldsymbol{S} \cdot \boldsymbol{I} \rangle / n|_{z=0}$ and $\mu_{\boldsymbol{S}\cdot\boldsymbol{I}}$ were obtained. Like the average hyperfine polarization data in Fig. 4, the values of the various quantities listed in Table I are also regionally specific rather than averaged over the entire cell surfaces. We also attempted to deduce $\mu_{\boldsymbol{S}\cdot\boldsymbol{I}}$ for a coated cell. However, the slope $\partial \langle \boldsymbol{S} \cdot \boldsymbol{I} \rangle / \partial n|_{z=0}$ and consequently $\mu_{\boldsymbol{S}\cdot\boldsymbol{I}}$ are too small to be reliably determined from our data.

In their study of the surface interactions of spin-polarized Na atoms, Grafström and Suter determined the normal gra-

TABLE I. The hyperfine polarization, its normal gradient, and normal gradient coefficient at the cell surface in three representative cells. In comparison, we note that the bulk hyperfine polarization in these three cells is 0.70 ± 0.02. The experimental conditions such as Rb density and pump beam intensity are given in the caption of Fig. 4.

Cell no.	$\langle \boldsymbol{S} \cdot \boldsymbol{I} \rangle|_{z=0}$	$\left. \frac{\partial \langle \boldsymbol{S} \cdot \boldsymbol{I} \rangle}{\partial n} \right\|_{z=0}$ (μm^{-1})	$\mu_{\boldsymbol{S}\cdot\boldsymbol{I}}$ (μm^{-1})
09	0.05	1.3	26
17	0.10	0.61	6.1
53	0.088	0.73	8.3

dient coefficient for the Zeeman polarization to be 0.51 μm^{-1} [16]. Their experimental method and experimental conditions being different from ours, it is difficult to compare their value of μ with ours. For example, their probing distance is much larger than the mean free path, whereas in our case the penetration depth of the probe beam is only a fraction of the mean free path. Therefore, the Na polarization in their case can be assumed to be an exponential function of the distance z from the cell surface, whereas in our case the diffusion equation may not be applicable and consequently the polarization is not necessarily an exponential function of z. This seems to be borne out by a simulation that we carried out, in which we assume the hyperfine polarization and consequently the population densities $N_a(z)$ and $N_b(z)$ near the surface can be described by simple exponential functions. We find that all the reflectivities $\mathcal{R}(\omega)$ measured at a number of different penetration depths d cannot be fitted well by the reflectivities calculated using such exponential population densities.

D. Experimental uncertainties

Because of the way the data are collected and analyzed in our experiment, the uncertainty in the average hyperfine polarization is relatively small. Some of the common causes of uncertainty such as Rb number density and laser intensity fluctuations have been greatly reduced. The Rb density is not obtained from the temperature readings but rather as a fitting parameter. Furthermore, it is the ratio N_F/N rather than the density N itself that is used in computing the polarization. The laser intensity fluctuations are canceled out in computing $\mathcal{R}(\omega)$. The scattering among the data taken in the same experimental setting due to the frequency drift of the pump beam is negligible. The main sources of uncertainty are due to the following: (i) the overlap between the pump and probe beams and the frequency setting of the pump beam, which may not be equally optimal in different experimental runs, (ii) the relatively poor signal-to-noise ratio when the penetration depth is very small, 0.3 μm for example, and (iii) the diffraction limited angular spread when the incidence angle is very close to the critical angle. Overall, we estimate the relative uncertainty in is between 5% and 10%.

III. CONCLUSIONS

We have studied the spatial variation of the regionally specific hyperfine polarization of Rb atoms in the vicinity ($\sim 10^{-5}$ cm of coated and uncoated Pyrex glass surfaces in optical pumping cells. The evanescent wave is used to probe the hyperfine polarization near the surface. Our results provide direct evidence that the hyperfine polarization near uncoated surfaces is significantly smaller than that in the bulk and that under our experimental conditions it decreases rapidly over a distance on the order of 10^{-3} cm. By contrast, in coated cells the hyperfine polarization remains constant as close to the surface as can be probed by our method, which is about 300 nm. We measure the average hyperfine polarization as a function of the penetration depth of the probe beam, from which we have been able to deduce regionally specific values of the hyperfine polarization, its normal gradient, and normal gradient coefficient $\mu_{\mathbf{S}\cdot\mathbf{I}}$ at the surface in three representative uncoated cells. We find that under our experimental conditions the Rb hyperfine polarization at the surface in uncoated cells is about 10% of the bulk hyperfine polarization.

ACKNOWLEDGMENTS

This work was partially supported by the Rutgers University Research Council. We wish to thank Professor Will Happer and Professor H. M. Lai for discussions. We also thank Steve Miller for his help in building a small chamber for independent control of the cell tip temperature.

APPENDIX

The general theory of wave propagation in a stratified medium was developed by Abelés [24]. Here we shall review the theory of reflection at the interface between a homogeneous medium and a stratified one [25]. Consider three media, to be referred to as the first, second, and third media. The first medium extends from $z=-\infty$ to $z=0$, the second from $z=0$ to $z=L$, and the third from $z=L$ to $z=\infty$. The first and third media are homogeneous. The first medium has a real dielectric constant ϵ_1, and the third one a complex dielectric constant $\epsilon_3=\epsilon_3'+i\epsilon_3''$. The magnetic permeabilities of all three media are assumed to be unity. Suppose a monochromatic plane wave, propagated in the first medium with a wave vector $\mathbf{k}^{(1)}$ in the xz plane making an angle of θ with the z axis, is incident on the interface (xy plane) between the first and second media.

1. A homogeneous medium

We shall first consider the case where the second medium is homogeneous. For TM or p-polarized incident waves, $H_x^{(1)}=H_z^{(1)}=0$. The tangential components of the magnetic and electric field vectors in the second medium can be written as, with the time dependence $\exp(-i\omega t)$ being omitted,

$$H_y^{(2)}(x,z) = U(z)\exp(ik_x^{(2)}x), \tag{A1}$$

$$E_x^{(2)}(x,z) = V(z)\exp(ik_x^{(2)}x), \tag{A2}$$

where $U(z)$ and $V(z)$ can be expressed in terms of their values at $z=0$ in a matrix form [25],

$$\begin{bmatrix} U(0) \\ V(0) \end{bmatrix} = \mathcal{M}(0,z)\begin{bmatrix} U(z) \\ V(z) \end{bmatrix}. \tag{A3}$$

Here

$$\mathcal{M}(0,z) = \begin{bmatrix} \cos(k_z^{(2)}z) & -i\dfrac{\epsilon_2 k_0}{k_z^{(2)}}\sin(k_z^{(2)}z) \\ -i\dfrac{k_z^{(2)}}{\epsilon_2 k_0}\sin(k_z^{(2)}z) & \cos(k_z^{(2)}z) \end{bmatrix} \tag{A4}$$

is the characteristic matrix, and $k_x^{(2)}$ and $k_z^{(2)}$ are, respectively, the x and z components of the wave vector $\mathbf{k}^{(2)}$ in the second medium. We have

$$k_x^{(2)} = k^{(2)} \sin\theta_2 = k_0\sqrt{\epsilon_1}\sin\theta, \tag{A5}$$

$$k_z^{(2)} = k^{(2)} \cos\theta_2 = k_0\sqrt{\epsilon_2 - \epsilon_1 \sin^2\theta}, \tag{A6}$$

where k_0 is the wave vector in the vacuum and θ_2 the angle between $\mathbf{k}^{(2)}$ and the z axis. We have used the law of refraction $\sqrt{\epsilon_2}\sin\theta_2 = \sqrt{\epsilon_1}\sin\theta$ in Eq. (A6). We note that $k_z^{(2)}$ is a complex number in the case of total internal reflection.

The matrix $\mathcal{M}$ for TE or s-polarized incident waves is

$$\mathcal{M}(0,z) = \begin{bmatrix} \cos(k_z^{(2)}z) & -i\dfrac{k_0}{k_z^{(2)}}\sin(k_z^{(2)}z) \\ -i\dfrac{k_z^{(2)}}{k_0}\sin(k_z^{(2)}z) & \cos(k_z^{(2)}z) \end{bmatrix}. \tag{A7}$$

2. A stratified medium

Now suppose that ϵ_2 is a function of z, i.e., the second medium is a stratified one. We want to relate the tangential components of the magnetic and electric fields at $z=0$ to those at $z=L$. For this purpose, we divide the second medium into N thin slices: $z_n \leqslant z \leqslant z_{n+1}$ $(n=0,1,\ldots,N-1)$, where $z_n = nL/N$. Each of these thin slices will be considered as homogeneous. Consider the nth slice located between z_n and z_{n+1}. The tangential components of the electric and magnetic fields at z_n and z_{n+1} are related by the $\mathcal{M}(z_n, z_{n+1})$ matrix,

$$\begin{bmatrix} U(z_n) \\ V(z_n) \end{bmatrix} = \mathcal{M}(z_n, z_{n+1}) \begin{bmatrix} U(z_{n+1}) \\ V(z_{n+1}) \end{bmatrix}, \tag{A8}$$

where

$$\mathcal{M}(z_n, z_{n+1}) = \begin{bmatrix} \cos[k_z^{(2)}(z_n)(z_{n+1}-z_n)] & -i\dfrac{\epsilon_2(z_n)k_0}{k_z^{(2)}(z_n)}\sin[k_z^{(2)}(z_n)(z_{n+1}-z_n)] \\ -i\dfrac{k_z^{(2)}(z_n)}{\epsilon_2(z_n)k_0}\sin[k_z^{(2)}(z_n)(z_{n+1}-z_n)] & \cos[k_z^{(2)}(z_n)(z_{n+1}-z_n)] \end{bmatrix}. \tag{A9}$$

Therefore,

$$\begin{bmatrix} U(0) \\ V(0) \end{bmatrix} = \prod_{n=0}^{N-1} \mathcal{M}(z_n, z_{n+1}) \begin{bmatrix} U(L) \\ V(L) \end{bmatrix}. \tag{A10}$$

In the limit $N \to \infty$, Eq. (A10) becomes

$$\begin{bmatrix} U(0) \\ V(0) \end{bmatrix} = \mathcal{M}(0,L) \begin{bmatrix} U(L) \\ V(L) \end{bmatrix}, \tag{A11}$$

where the characteristic matrix $\mathcal{M}(0,L)$ is

$$\mathcal{M}(0,L) = \lim_{N\to\infty} \prod_{n=0}^{N-1} \mathcal{M}(z_n, z_{n+1}). \tag{A12}$$

Now we consider the boundary conditions at $z=0$ and $z=L$. Let A and R represent the complex amplitude of the magnetic vector of the incident and reflected waves in the first medium and T that of the transmitted wave in the third medium. The boundary conditions at $z=0$ are

$$A + R = U(0), \tag{A13}$$

$$p_1(A - R) = V(0), \tag{A14}$$

and at $z=L$ are

$$U(L) = T, \tag{A15}$$

$$V(L) = p_3 T, \tag{A16}$$

where

$$p_1 = \frac{1}{\sqrt{\epsilon_1}}\cos\theta, \tag{A17}$$

$$p_3 = \frac{1}{\epsilon_3}\sqrt{\epsilon_3 - \epsilon_1 \sin^2\theta}. \tag{A18}$$

Since the values $U(0), V(0)$ and $U(L), V(L)$ are related by the $\mathcal{M}$ matrix, we obtain from Eqs. (A11)–(A16) the reflection coefficient

$$r = \frac{(m_{11} + m_{12}p_3)p_1 - (m_{21} + m_{22}p_3)}{(m_{11} + m_{12}p_3)p_1 + (m_{21} + m_{22}p_3)}, \tag{A19}$$

where the matrix elements m_{ij} are given by Eq. (A12). The reflectivity $\mathcal{R}$ is given by

$$\mathcal{R} = |r|^2. \tag{A20}$$

For TE or s-polarized incident waves, the characteristic matrix $\mathcal{M}$ is

$$\mathcal{M}(0,L) = \lim_{N\to\infty} \prod_{n=0}^{N-1} \mathcal{M}(z_n, z_{n+1}), \tag{A21}$$

where

$$\mathcal{M}(z_n, z_{n+1}) = \begin{bmatrix} \cos[k_z^{(2)}(z_n)(z_{n+1}-z_n)] & -i\dfrac{k_0}{k_z^{(2)}(z_n)} \sin[k_z^{(2)}(z_n)(z_{n+1}-z_n)] \\ -i\dfrac{k_z^{(2)}(z_n)}{k_0} \sin[k_z^{(2)}(z_n)(z_{n+1}-z_n)] & \cos[k_z^{(2)}(z_n)(z_{n+1}-z_n)] \end{bmatrix}. \tag{A22}$$

The reflection coefficient is still given by Eq. (A19) except that the matrix elements m_{ij} are now given by Eqs. (A21) and (A22), and

$$p_1 = \sqrt{\epsilon_1}\cos\theta, \tag{A23}$$

$$p_3 = \sqrt{\epsilon_3 - \epsilon_1 \sin^2\theta}. \tag{A24}$$

3. Fresnel formulas

We consider the special case where the second medium is homogeneous and $\epsilon_2 = \epsilon_3$. In this case, the problem becomes the reflection at the interface ($z=0$) between two homogeneous media, and we expect the reflection coefficient or reflectivity to be the same as that given by the Fresnel formulas. The characteristic matrix $\mathcal{M}$ becomes

$$\mathcal{M}(0,L) = \begin{bmatrix} \cos(k_z^{(2)}L) & -i\dfrac{\epsilon_2 k_0}{k_z^{(2)}} \sin(k_z^{(2)}L) \\ -i\dfrac{k_z^{(2)}}{\epsilon_2 k_0} \sin(k_z^{(2)}L) & \cos(k_z^{(2)}L) \end{bmatrix} \tag{A25}$$

for TM or *p*-polarized waves, and

$$\mathcal{M}(0,L) = \begin{bmatrix} \cos(k_z^{(2)}L) & -i\dfrac{k_0}{k_z^{(2)}} \sin(k_z^{(2)}L) \\ -i\dfrac{k_z^{(2)}}{k_0} \sin(k_z^{(2)}L) & \cos(k_z^{(2)}L) \end{bmatrix} \tag{A26}$$

for TE or *s*-polarized waves. Substituting Eqs. (A17), (A18), and (A25) in Eq. (A19), we obtain

$$r = \frac{\dfrac{\epsilon_2}{\epsilon_1}\cos\theta - \sqrt{\dfrac{\epsilon_2}{\epsilon_1} - \sin^2\theta}}{\dfrac{\epsilon_2}{\epsilon_1}\cos\theta + \sqrt{\dfrac{\epsilon_2}{\epsilon_1} - \sin^2\theta}}, \tag{A27}$$

which is the Fresnel formula for *p*-polarized incident waves. Similarly, we have for *s*-polarized incident waves

$$r = \frac{\cos\theta - \sqrt{\dfrac{\epsilon_2}{\epsilon_1} - \sin^2\theta}}{\cos\theta + \sqrt{\dfrac{\epsilon_2}{\epsilon_1} - \sin^2\theta}}. \tag{A28}$$

4. Numerical calculations of $\mathcal{R}(\omega)$, $\mathcal{T}(\omega)$, d_ω, and $\overline{\langle \boldsymbol{S}\cdot\boldsymbol{I}\rangle}$

a. Reflectivity $\mathcal{R}(\omega)$

The numerical calculation of the reflectivity $\mathcal{R}(\omega)$ at the interface between the Pyrex glass and Rb vapor requires knowledge of the dielectric constant of the Pyrex glass (first medium) and that of the Rb vapor near the surface (second medium). The determination of each of these quantities is discussed in the following.

(i) Dielectric constant ϵ_1 of the Pyrex glass. The dielectric constant ϵ_1 of the Pyrex glass is obtained from the critical angle $\bar{\theta}_c$, which in turn is determined as follows [20]. We tune the frequency of the probe beam far away from the Rb $D1$ line so that the dielectric constant of the Rb vapor can be safely regarded as unity. The critical angle $\bar{\theta}_c$ then corresponds to the onset of the total internal reflection of the probe beam, which manifests itself as a sudden change in the intensity of the reflected beam. The error associated with this method of determining $\bar{\theta}_c$ is of the order of the diffraction limit of the probe laser beam. The dielectric constant ϵ_1 of the Pyrex glass is given by $\epsilon_1 = 1/\sin^2\bar{\theta}_c$.

(ii) Dielectric constant ϵ_2 of the Rb vapor near the surface. The complex dielectric constant of the Rb vapor near the cell surfaces is given by the following equation [13,14]:

$$\epsilon_2(\omega) = 1 + \frac{2\pi e^2}{m_e}\sum_{FF'} \frac{f_{FF'}N_F}{\omega_{FF'}} \int_{-\infty}^{\infty} dv_x W(v_x) \left[2\int_{-\infty}^{0} dv_z W(v_z) \frac{1}{\omega_{FF'} - \omega + k_x^{(2)}v_x + k_z^{(2)}v_z - i\gamma_{FF'}/2} \right], \tag{A29}$$

where e and m_e are the electric charge and mass of the electron, N_F is the population in the ground-state hyperfine multiplet F, and v_x and v_z are, respectively, the x and z components of the velocity of the atom. The normalized Maxwellian velocity distributions of v_x and v_z are given by

$$W(v_i) = \sqrt{\frac{M}{2\pi k_B T}} \exp\left(-\frac{Mv_i^2}{2k_B T}\right) \quad (i = x,z), \quad \text{(A30)}$$

where k_B is the Boltzmann constant, T is the temperature of the vapor, and M is the mass of the Rb atom. The transition frequencies $\omega_{FF'}$ are given in Ref. [21]. Collisions of Rb atoms with N_2 molecules and surfaces, however, cause a shift in the frequencies $\omega_{FF'}$ [12,26]. The homogeneous broadening $\gamma_{FF'}$ includes natural broadening and broadening due to collisions with N_2 [26], Rb [27], and surfaces [28]. The oscillator strengths $f_{FF'}$ for transitions between ground-state and excited-state hyperfine multiplets are related to the electronic oscillator strength f by

$$f_{FF'} = fW^2(J'F'JF;I1)(2J+1)(2F'+1), \quad \text{(A31)}$$

where W is the Racah coefficient, J and J' are the total electronic angular momentum of the ground state $5\,^2S_{1/2}$ and the excited state $5\,^2P_{1/2}$, respectively, and $f=0.35$ is the oscillator strength of the Rb D1 line. The summation in Eq. (A29) is over all the transitions $F \to F'$ of the D1 line of ^{87}Rb and ^{85}Rb atoms (see Fig. 2). For cells filled with isotopically enriched Rb (98.3 at. % ^{87}Rb), the summation over the ^{85}Rb transitions can be neglected unless absorption due to ^{85}Rb is not negligible, e.g., at high cell temperatures. In Eq. (A29), we used the fact that the contribution to the reflectivity from Rb atoms flying away from the surface is the same as that from the Rb atoms flying towards the surface [13,14].

For total internal reflection, the x and z components of the wave vector in the vapor are given by

$$k_x^{(2)} = \sqrt{\epsilon_1}\sin\theta\, k_0 = \zeta k_0, \quad \text{(A32)}$$

$$k_z^{(2)} \approx i\sqrt{\epsilon_1 \sin^2\theta - 1}k_0 = i\xi k_0. \quad \text{(A33)}$$

Equation (A33) is obtained from Eq. (A6) by using the zeroth-order approximation for ϵ_2, i.e., by setting $\epsilon_2=1$. Therefore, the $k_x^{(2)}v_x$ term in Eq. (A29) is equivalent to a frequency shift (Doppler shift) and the $k_z^{(2)}v_z$ term a broadening (transit time broadening). In our numerical calculation, we use the following greatly simplified expression for ϵ_2:

$$\epsilon_2(\omega) = 1 + \frac{2\pi e^2}{m_e}\sum_{FF'}\frac{f_{FF'}N_F}{\omega_{FF'}}\int_{-\infty}^{\infty} dv_x W(v_x) \times \frac{1}{\omega_{FF'} - \omega + \zeta k_0 v_x - i(\gamma_{FF'} + \gamma')/2}. \quad \text{(A34)}$$

The physical meaning of the simplification that leads to Eq. (A34) is that even though transit time broadening is not homogeneous because it depends on the velocity component v_z normal to the cell surface, we treat it as a homogeneous broadening γ', i.e., we use an average transit time broadening for all the v_z components. The broadening γ' depends on the penetration depth d, and is determined as a fitting parameter. By changing the integration variable to Doppler shift $\omega_x = \zeta k_0 v_x$, Eq. (A34) can also be written as

$$\epsilon_2(\omega) = 1 + \frac{2\pi e^2}{m_e}\sum_{F,F'}\frac{f_{FF'}N_F}{\omega_{FF'}}\int_{-\infty}^{\infty} d\omega_x \frac{1}{\sqrt{\pi}\Delta_x} \times \exp\left(-\frac{\omega_x^2}{\Delta_x^2}\right)\frac{1}{\omega_{FF'} - \omega + \omega_x - i\gamma/2}, \quad \text{(A35)}$$

where $\gamma = \gamma_{FF'} + \gamma'$ is the total homogeneous broadening and the linewidth parameter Δ_x is given by

$$\Delta_x = \zeta k_0 \sqrt{\frac{2k_B T}{M}}. \quad \text{(A36)}$$

We have assumed that collisional broadening, which is the dominant contribution to $\gamma_{FF'}$, is the same for all the transitions $F \to F'$, and therefore $\gamma_{FF'}$ is approximately independent of F and F'.

We find that Eq. (A29) and Eq.(A34) or Eq. (A35) give an almost equally good fit to the experimental data. When the pump beam is on, the population density N_F depends on the distance from the cell surface as a result of hyperfine pumping and surface relaxation. Furthermore, depending on the pump beam intensity, there may be a certain degree of saturation. Therefore, we use the following expression for ϵ_2 during hyperfine pumping:

$$\epsilon_2(\omega,z) = 1 + \frac{2\pi e^2}{m_e}\sum_{F,F'}\frac{f_{FF'}}{\omega_{FF'}}\left[N_F(z) - \frac{g_F}{g_{F'}}N_{F'}(z)\right] \times \int_{-\infty}^{\infty} d\omega_x \frac{1}{\sqrt{\pi}\Delta_x}\exp\left(-\frac{\omega_x^2}{\Delta_x^2}\right)\frac{1}{\omega_{FF'} - \omega + \omega_x - i\gamma/2}. \quad \text{(A37)}$$

That is, the Rb vapor near the surface needs to be treated as a stratified medium.

(iii) Numerical calculation of $\mathcal{R}(\omega)$. The calculation of the reflectivity $\mathcal{R}(\omega)$ depends on whether the pump beam is on or off. When the pump beam is off, the Rb vapor near the surface can be treated as a homogeneous medium with a complex dielectric constant, whereas when the pump beam is on, the Rb vapor near the surface needs to be treated as a stratified medium. More detailed discussion follows.

When the pump beam is off, we can assume that $N_{F'}=0$, the saturation due to the probe beam being negligible. Optical pumping due to the probe beam is also negligible. Therefore, the Rb atoms are equally distributed among all the magnetic sublevels of the ground state. That is, we have

$$N_F = \frac{2F+1}{(2J+1)(2I+1)}\eta N, \quad \text{(A38)}$$

where η is the isotopic abundance of the two Rb isotopes and N is the Rb number density. We also assume that N_F does not depend on the distance z from the surface. The Rb vapor near the surface can thus be treated as a homogeneous medium with a complex dielectric constant $\epsilon_2(\omega)$, which is given by Eq. (A35), and the reflectivity $\mathcal{R}(\omega)$ for a p-polarized incident wave is obtained from the Fresnel formula Eq. (A27).

When the pump beam is on, the population $N_{F'}$ in the excited-state hyperfine multiplet F' may not be negligible due to the saturation effect. We assume that the two hyperfine multiplets $F'=I-1/2$ and $F'=I+1/2$ of the excited state $5\,^2P_{1/2}$ are populated according to their statistical weights, and therefore we have

$$\frac{N_{F'}}{g_{F'}}=\frac{N_e}{g_e}, \tag{A39}$$

where N_e is the total population and $g_e=4I+2$ the total statistical weight of the excited states $5\,^2P_{1/2}$. Since the Rb population densities N_F near the surface depend on the distance z from the surface, the Rb vapor in the vicinity of surfaces needs to be treated as a stratified medium, and its dielectric constant ϵ_2 is given by Eq. (A37). The reflectivity $\mathcal{R}(\omega)$ can be calculated using Eq. (A19). For example, in the case of hyperfine pumping of ^{87}Rb atoms, if we use $\tilde{N}_a(z)$ and $\tilde{N}_b(z)$ as the population densities in Eq. (A37) and we treat the Rb vapor from $z=0$ to $z=L$ as the second medium and the Rb vapor beyond $z=L$ as the third medium, whose dielectric constant ϵ_3 is given by Eq. (A35) with N_F and N_e being equal to the bulk values, the reflectivity $\mathcal{R}(\omega)$ is then calculated using Eqs. (A9), (A12), and (A17)–(A20). In evaluating the characteristic matrix $\mathcal{M}$, we find it adequate to use $\Delta z=0.05$ μm in Eq. (A9).

b. Transmissivity $\mathcal{T}(\omega)$

The transmissivity $\mathcal{T}(\omega)$ of the probe beam is given by

$$\mathcal{T}(\omega)=\exp\left[-\frac{2\pi\epsilon_2'' l}{\lambda_0}\right], \tag{A40}$$

where

$$\epsilon_2''(\omega)=1+\frac{2\pi e^2}{m_e}\sum_{FF'}\frac{f_{FF'}}{\omega_{FF'}}\left[N_F-\frac{g_F}{g_{F'}}N_{F'}\right]\times\int_{-\infty}^{\infty}dv_z W(v_z)\frac{\gamma/2}{(\omega_{FF'}-\omega+k_0v_z)^2+\gamma^2/4} \tag{A41}$$

is the imaginary part of the dielectric constant of the Rb vapor in the bulk and l is the optical path length. In computing the transmissivity, we can safely neglect the contribution from the stratified surface layer and treat the Rb vapor as a homogeneous medium. Due to the long path length, even in cells filled with isotopically enriched Rb (98.3 at. % ^{87}Rb), the contribution from ^{85}Rb atoms needs to be taken into account in calculating the transmissivity $\mathcal{T}(\omega)$.

c. Penetration depth d_ω

The penetration depth d_ω is defined to be the distance where the amplitude of the evanescent wave decays to $1/e$ of its value. For a homogeneous medium, this $1/e$ decay distance is the same for the electric and magnetic fields, and is given by Eq. (6). For a stratified medium, however, this $1/e$ decay distance is not necessarily the same for the electric and magnetic fields. For a TM or p-polarized probe beam, we have, from Eq. (A11),

$$U(d_\omega)=m_{11}^{-1}U(0)+m_{12}^{-1}V(0), \tag{A42}$$

where m_{ij}^{-1} are the matrix elements of the inverse of the characteristic matrix $\mathcal{M}(0,d_\omega)$. Thus

$$\frac{U(d_\omega)}{U(0)}=m_{11}^{-1}+m_{12}^{-1}\frac{V(0)}{U(0)}. \tag{A43}$$

From Eqs. (A13) and (A14), we have

$$\frac{V(0)}{U(0)}=p_1\frac{1-r}{1+r}. \tag{A44}$$

By definition, $|U(d_\omega)/U(0)|=1/e$. Thus we have

$$\frac{1}{e}=\left|m_{11}^{-1}+m_{12}^{-1}p_1\frac{1-r}{1+r}\right|. \tag{A45}$$

Equation (A45) determines the penetration depth d_ω for the magnetic field for a TM probe beam. Similarly, we can show that the penetration depth d_ω for the electric field is determined by the following equation:

$$\frac{1}{e}=\left|\sqrt{\frac{\epsilon_2(d_\omega)}{\epsilon_2(0)}}\left(m_{22}^{-1}+\frac{m_{21}^{-1}}{p_1}\frac{1+r}{1-r}\right)\right|. \tag{A46}$$

The difference between the penetration depth for the electric field and that for the magnetic field is illustrated in Fig. 7(a). Similar equations can be obtained for TE probe beams.

d. Average hyperfine polarization $\overline{\langle \boldsymbol{S}\cdot\boldsymbol{I}\rangle}$

To determine the average hyperfine polarization $\overline{\langle \boldsymbol{S}\cdot\boldsymbol{I}\rangle}$ near the surface, we measure the reflectivities $\mathcal{R}(\omega)$ when the pump beam is on and off and compare them with the calculated ones. As discussed in Appendix A 4 a, when the pump beam is off, the reflectivity $\mathcal{R}(\omega)$ is calculated using Eq. (A27), with $\epsilon_2(\omega)$ being given by Eq. (A35). We adjust the fitting parameters to achieve the best fit between the measured and calculated reflectivities. The fitting parameters are the Rb number density N and the homogeneous linewidth γ. The best fit yields the values of N and γ. By subtracting the homogeneous broadening $\gamma_{FF'}$, which includes natural broadening and collisional broadening due to N_2, Rb, and surfaces from γ, one obtains the value of the average transit time broadening γ', which is found to range from 10 to 160 MHz for the penetration depths used in our study [15]. However, we note that the uncertainties in $\gamma_{FF'}$ that are associated with various collisional broadening cannot be separated in the fitting process from the average transit time broadening γ'. Therefore, the average transit time broadening γ' obtained this way will contain the uncertainties of other homogeneous broadening. When the pump beam is on, the population densities N_a, N_b, and N_e in the vicinity of surfaces are functions of z due to surface relaxation; and therefore the dielectric constant ϵ_2 of the Rb vapor near the surface is given by Eq. (A37). In computing the average hyperfine polarization $\overline{\langle \boldsymbol{S}\cdot\boldsymbol{I}\rangle}$, we replace the z-dependent population densities in Eq. (A37) by their average values $\overline{N_a}$,

$\overline{N_b}$, and $\overline{N_e}$, so that the Rb vapor near the surface can be treated as homogeneous and the reflectivity $\mathcal{R}(\omega)$ can therefore be calculated using the Fresnel formula Eq. (A27). We use $\overline{N_a}-(g_a/g_e)\overline{N_e}$ and $\overline{N_b}-(g_b/g_e)\overline{N_e}$ as fitting parameters, which are adjusted to give the best fit between the measured reflectivity $\mathcal{R}(\omega)$ and the calculated one. The values of $\overline{N_a}$ and $\overline{N_b}$ are then obtained using the relation $\overline{N_a}+\overline{N_b}+\overline{N_e}=N$. Since $\overline{N_e}$ accounts for no more than a few percent of the total population, the power broadening is neglected in the numerical calculation and we use the same fitting parameter γ when the pump beam is on and off.

The average bulk hyperfine polarization is obtained from the bulk values of the ground-state hyperfine multiplet populations $N_a^{(0)}$ and $N_b^{(0)}$, which are determined from the transmissivity $\mathcal{T}(\omega)$ of the probe beam. We compare the measured transmissivity when the pump beam is off with the calculated one to determine the number densities of ^{87}Rb and ^{85}Rb. The values of $N_a^{(0)}$ and $N_b^{(0)}$ when the pump beam is on are determined as fitting parameters that give the best fit between the measured transmissivity when the pump beam is on and the calculated one, using the same values of the Rb number densities that are determined when the pump beam is off.

[1] P. L. Bender, E. C. Beaty, and A. R. Chi, Phys. Rev. Lett. **1**, 311 (1958); W. E. Bell and A. L. Bloom, Phys. Rev. **109**, 219 (1958); M. Arditi and T. R. Carver, *ibid.* **109**, 1012 (1958); A. Moretti and F. Strumia, Phys. Rev. A **3**, 349 (1971); N. Beverini, P. Minguzzi, and F. Strumia, *ibid.* **4**, 550 (1971); N. N. Yakobson, Opt. Spectrosc. **37**, 225 (1974).

[2] See, for example, Jacques Vanier and Claude Audoin, *The Quantum Physics of Atomic Frequency Standards* (Adam Hilger, Philadelphia, 1989).

[3] H. G. Robinson, E. S. Ensberg, and H. G. Dehmelt, Bull. Am. Phys. Soc. **3**, 9 (1958); C. O. Alley, in *Advances in Quantum Electronics*, edited by J. R. Singer (Columbia University Press, New York, 1961), p. 120.

[4] D. Budker, D. F. Kimball, S. M. Rochester1, V. V. Yashchuk1, and M. Zolotorev, Phys. Rev. A **62**, 043403 (2000).

[5] M. S. Albert, G. D. Cates, B. Driehuys, W. Happer, C. S. Springer, Jr., B. Saam, and A. Wishnia, Nature (London) **370**, 199 (1994).

[6] M. A. Bouchiat and J. Brossel, Phys. Rev. **147**, 41 (1966).

[7] X. Zeng, E. Miron, W. A. van Wijngaarden, D. Schreiber, and W. Happer, Phys. Lett. **96**, 191 (1983).

[8] Z. Wu, W. Happer, M. Kitano, and J. Daniels, Phys. Rev. A **42**, 2774 (1990).

[9] K. Zhao and Z. Wu, Phys. Rev. Lett. **91**, 113003 (2003).

[10] K. Zhao and Z. Wu, Phys. Rev. A **70**, 010901(R) (2004).

[11] V. G. Bordo, J. Loerke, and H. G. Rubahn, Phys. Rev. Lett. **86**, 1490 (2001).

[12] M. Chevrollier, M. Fichet, M. Oria, G. Rahmat, D. Bloch, and M. Ducloy, J. Phys. II **2**, 631 (1992).

[13] G. Nienhuis, F. Schuller, and M. Ducloy, Phys. Rev. A **38**, 5197 (1988).

[14] F. Schuller, G. Nienhuis, and M. Ducloy, Phys. Rev. A **43**, 443 (1991).

[15] P. Simoneau and M. Ducloy, Opt. Commun. **59**, 103 (1986).

[16] S. Grafström and D. Suter, Z. Phys. D: At., Mol. Clusters **38**, 119 (1996); Phys. Rev. A **54**, 2169 (1996).

[17] Z. Wu, S. Schaefer, G. D. Cates, and W. Happer, Phys. Rev. A **37**, 1161 (1988).

[18] F. Masnou-Seeuws and M. Bouchiat, J. Phys. (Paris) **28**, 406 (1967).

[19] X. Zeng, Z. Wu, T. Call., E. Miron, D. Schreiber, and W. Happer, Phys. Rev. A **31**, 260 (1985).

[20] K. Zhao, Z. Wu, and H. M. Lai, J. Opt. Soc. Am. B **18**, 1904 (2001).

[21] G. P. Barwood, P. Gill, and W. R. C. Rowley, Appl. Phys. B: Photophys. Laser Chem. **53**, 142 (1991).

[22] W. W. Quivers, Phys. Rev. A **34**, 3822 (1986).

[23] E. H. Kennard, *Kinetic Theory of Gases* (McGraw-Hill, New York, 1938).

[24] F. Abelés, Ann. Phys. (Paris) **5**, 596 (1950); **5**, 706 (1950).

[25] Max Born and Emil Wolf, *Principles of Optics*, 6th ed. (Pergamon Press, New York, 1980).

[26] M. V. Romalis, E. Miron, and G. D. Cates, Phys. Rev. A **56**, 4569 (1997).

[27] K. Niemax and G. Pichler, J. Phys. B **8**, 179 (1975).

[28] M. Gorris-Neveux, P. Monnot, M. Fichet, M. Ducloy, R. Barb, and J. C. Keller, Opt. Commun. **134**, 85 (1997).